Korean Journal of Remote Sensing, Vol.18, No.1, 2002, pp.13~23

Change Detection of Land-cover from Multi-temporal KOMPSAT-1 EOC Imageries

Sung-Ryong Ha, Byung-Woon Ahn, and Sang-Young Park

Department of Urban Engineering, Chungbuk National University

Abstract : A radiometric correction method is developed to apply multi-temporal KOMPSAT-1 EOC satellite images for the detection of land-cover changes by recognizing changes in reflection pattern. Radiometric correction was carried out to eliminate the atmospheric effects that could interfere with the image property of the satellite data acquired at different multi-times. Four invariant features of water, sand, paved road, and roofs of building are selected and a linear regression relationship among the control set images is used as a correction scheme. It is found that the utilization of panchromatic multi-temporal imagery requires the radiometric scene standardization process to correct radiometric errors that include atmospheric effects and digital image processing errors. Land-cover with specific change pattern such as paddy field is extracted by seasonal change recognition process.

Key Words : KOMPSAT, Standardization, Multi-temporal, Change Detection, Paddy Field.

1. Introduction

Remotely sensed image is broadly used to monitor changes in land surface conditions. Many change detection methods have been proposed and applied, many of which are reviewed by Singh (1989). Methods of change detection in remote sensing typically analyze sequential images of the same area and involve the detection and display of the changes in the image space. The underlying assumption in using remotely sensed data for change detection is that changes in the land-cover result in significant differences in the remote sensing measurements between two or more dates. In addition, these differences must be larger or somehow distinguishable from other changes in the images due to changing atmospheric conditions, seasons, illumination conditions, and sensor calibration.

Comparison of images taken on different dates has been the subject of a large number of programs (Badwahr *et al.*, 1982; Teiller *et al.*, 1987; Schott *et al.*, 1988; Hall *et al.*, 1991; Coppin *et al.*, 1994; Collins *et al.*, 1996). In particular, Badwahr (1982) dealt with the problem of multi-temporal classification of crops and defined the spectral profile as an analytic description of the spectral response of scene element. Some works by Teillet *et al.* (1987) described the use of a dynamic regression algorithm for incorporating atmospheric models into image correction procedures. Many other techniques rely on in-scene or ground truth elements to independently normalize individual images for temporal variations (Fehrenbach, 1983; Piech *et al.*, 1978; Piech

Received 25 January 2002; Accepted 28 January 2002.

and Scott, 1974). Multi-temporal image normalization method by linear transform was applied in some works (Collins and Woodcock, 1996; Coppin and Bauer, 1994; Hall *et al.*, 1991; Schott *et al.*, 1988).

Lee and Kim (2000) studied on the monitoring of deforested area by visual interpretation and computer classification of EOC data. Considering the limitation of using single panchromatic data, visual interpretation seems to be an appropriate approach. It is mentioned that the possible effects of the pixel value variations due to data acquisition environments, such as the atmospheric condition, sensor calibration and different growing stage of vegetation, should be minimized in analyzing multi-temporal satellite data sets.

It is a difficult task to visually compare two automated fashions of scenes acquired from the same target on different dates. This difficulty comes from the temporal variations of atmospheric conditions, look/view angles, or sensor parameters. Many techniques have been developed to account for non-scene-dependent changes in image appearance by removing most of the effects of sun zenith angle, sensor response, and atmospheric variations from two or more temporally disunited images.

Temporal images are suitable for various applications as if those have been taken under identical acquisition conditions by excluding external effects. This operation has been termed "temporal image standardization." A statistical regression approach has been used to standardize the satellite data over time. Preference is given to a technique based on spatially well-defined and spectrally and radiometrically stable features (Caselles and Garcia, 1989). On the other hand, temporal image standardization needs a control set, i.e., sets of scene landscape elements with a mean reflectance that is expected to change little with time (Hall *et al.*, 1991). For instance, road, roof, and paved square are usually considered as a control set.

The main objective of this paper is to detect change area from annual imagery and to extract paddy field from seasonally collected EOC images. Annual change detection was performed on two images acquired on the March 2000 and 2001 respectively. Paddy field was extracted from the images acquired on March and June 2001.

2. Data Description

Study area is located nearby Daechung Reservoir that lays over Chungbuk province and Chungnam province, Korea (Fig. 1). This site consists of forest area, agricultural, and a few of urbanized area and stream. Miho-stream runs through the study area and cultivated area surrounds the stream. Most of area is used for paddy cropping and rarely used for other cropping purpose, for instance, vegetables with cropping facility.

KOMPSAT-1 (Korea multi-purpose satellite) was launched on 21 December 1999 by KARI (Korea Aerospace Research Institute). The EOC (Electro optical camera), a payload of KOMPSAT-1 provides panchromatic satellite imagery with 6.6m ground resolution and 17km swath (Satellite Application Group, 1999). This study used the remotely sensed data obtained on 1 March 2000, 18 March 2001 and 8 June 2001 by KOMPSAT-1 EOC. Unfortunately, the data acquired on June 2001 has no data on the description of image information about acquisition environment, due to the error at that time of transferring to receiving station from satellite.

3. Methodology

1) Pre-processing

Pre-processing phase consists of image mosaic and geometric correction.

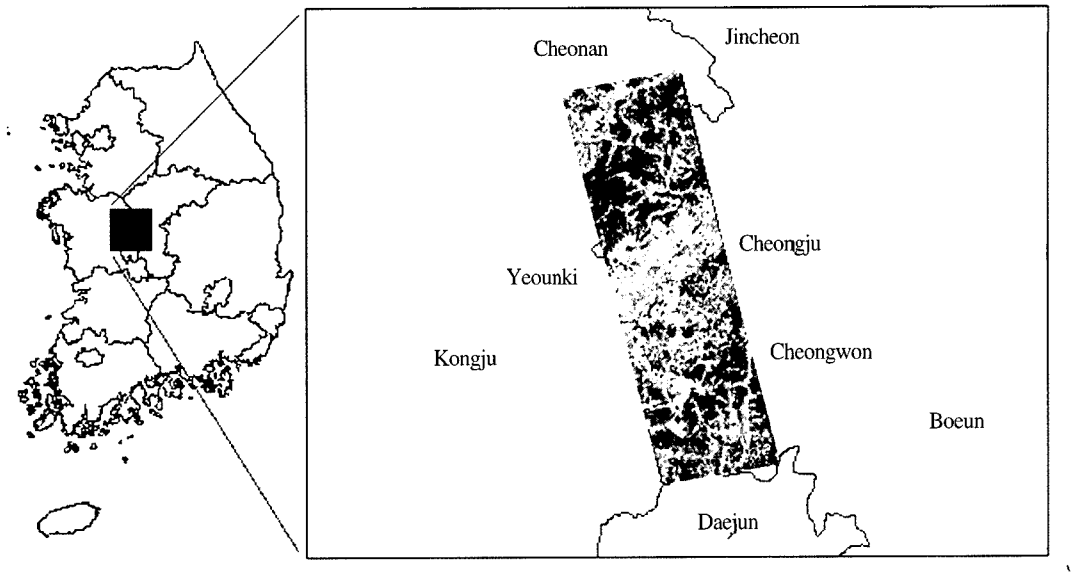

Fig. 1. Index map of the study region and EOC imagery.

Table 1. List of satellite data used and description.

Date	GRS*1	Scene ID
1 March, 2000	(928, 1325)	EOC_092813252000030101520 2P04_1R
	(928, 1326)	EOC_092813262000030101520 4P04_1R
	(928, 1327)	EOC_092813272000030101520 6P04_1R
18 March, 2001	(927, 1325)	EOC_092713252001031801551 3P03_1R
	(927, 1326)	EOC_092713262001031801551 4P03_1R
	(927, 1327)	EOC_092713272001031801551 6P03_1R
2 June, 2001*2	–	–
		–
		–

*1 GRS(Ground Reference System) is the reference coordinate system for KOMPSAT-EOC.
*2 Scene by pass 7724 has no scene information because of transfer failure at the acquisition date.

Image processing for producing a mosaic image was conducted using a pixel-based method. Three scenes of KOMSAT-1 EOC images acquired on different dates were used to make a scene of mosaic image. The Transverse Mercator (TM) projection scheme was applied to make a projected image because the original satellite image was taken as a simple image without reference coordination system. The image-to-map registration scheme was applied to rectify the image acquired on March 2000 whereas the image-to-image registration scheme was applied to the images acquired in 2001. A digital map prepared previously was used to collect the sixteen GCPs (ground truth points) for the rectification of the projected image of 2000. Twelve to sixteen GCPs for rectifying the projected images of 2001 were collected from the rectified image using image-to-map. A first-order, six-parameter, affine transformation method was applied to rectification. Using nearest-neighbor interpolation resampling logic, by which a digital number could be approximated for the original location of rectified pixel, the projected image was transformed to the rectified image that

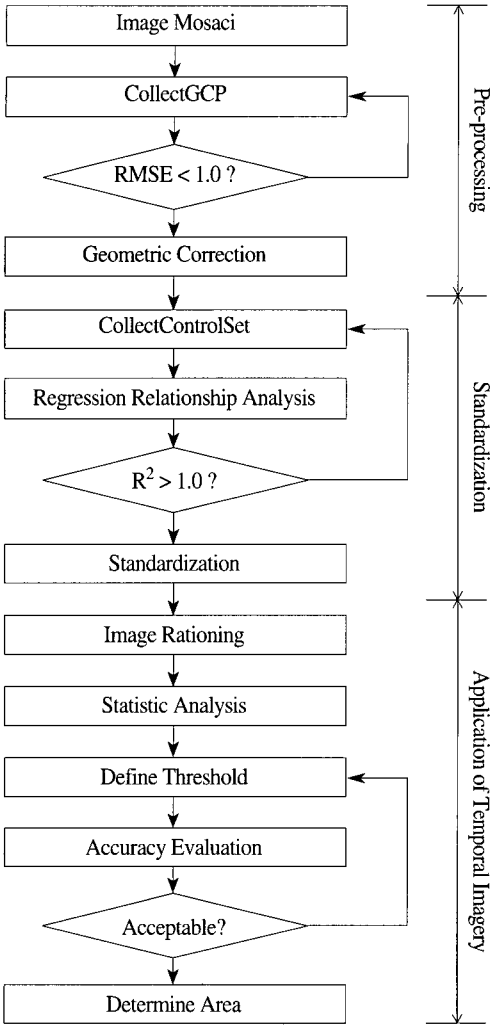

Fig. 2. Flow chart of KOMPSAT-1 EOC imagery application.

possessed the reference coordinate system.

2) Standardization

This paper employed a relative radiometric normalization process as a temporal image standardization method. This normalization uses a control set of the land covers, which are spectrally invariant features along the seasons of data acquisition. The extent of seasonal reflectance of the features was mainly considered for selecting the control set. In this paper, the four features of sand, road, roof, and water were selected to compose the control set. The sample number of control set features for sand, water, road, and roof was 503, 300, 419, and 400 pixels, respectively. They were collected from spatially identical locations using three different date images.

The standardization equation determined by the regression analysis is formulated by Eq. (1).

$$DN_{Date1} \cong DN^{T}_{Date2} = X \cdot DN_{Date2} + Y \quad (1)$$

where, *Date 1* and *Date 2* mean the date on which satellite images were acquired. The superscription, T means the image standardized, and X and Y denote the parameters determined by the regression analysis of the control set.

3) Application of Temporal Imagery

The image rationing method, which is one of the change detection methods, was used to discriminate the extent of image changed temporally. It produces the change image (CI), which indicates the change rate between acquisition dates. In addition, statistical analysis is necessary to define the threshold, by which the change of image is decided. The value of threshold is based on two statistics such as mean and standard deviation of the change image (CI). The image rationing method simplify can be expressed as follows.

$$CI = \frac{DN_{Date1} - DN_{Date2}}{DN_{Date1} + DN_{Date2}} \quad (2)$$

In this study, two kinds of analysis were conducted to detect the temporal change of image normalized. One was the annual change detection and the other one was the seasonal change analysis.

The annual change detection needs seasonally identical imagery in order to minimize the change resulted from seasonal difference. Therefore, two standardized images, acquired on March 2000 and March 2001, were used to detect the annual change of image. The image rationing method was applied to generate the change images of two standardized images.

Table 2. Summary of the basic statistic of the control sets.*5

Date	March 1, 2000				March 18, 2001				June 2, 2001			
Feature	Sand	Water	Road	Roof	Sand	Water	Road	Roof	Sand	Water	Road	Roof
Min.*4	73	42	50	54	80	52	61	64	105	41	63	68
Max.*4	103	45	59	58	107	57	75	71	151	54	87	83
Avg.*4	93.32	43.39	53.53	55.98	97.54	54.18	66.23	68.96	137.7	47.73	76.16	79.06
Stdev*1.	4.96	0.64	1.61	0.71	4.37	1.32	2.16	0.81	8.09	4.55	3.73	1.79
Skew*2.	-0.7	-0.27	0.32	0.07	-0.48	-0.01	0.29	-0.53	-1.03	-0.26	0.18	-0.58
Kurt.*3	0.50	-0.42	0.61	-0.16	0.35	-1.11	-0.01	3.37	1.08	-1.43	0.07	3.41

*1 Stdev. means a standard deviation of digital numbers observed.

*2 Skew. means a skewness coefficient defined by: $Skew = (1/N) \times \sum_{p=1}^{N} ((DN_p - \mu)/\sigma)^3$.

*3 Kurt. means a kurtosis defined by: $Kurt = [(1/N) \times \sum_{p=1}^{N} ((DN_p - \mu)/\sigma)^4] - 3$.

*4 Min., Max., and Avg. mean the value of minimum, maximum, and average, respectively.

*5 Number of pixel used to control set in terms of sand, water, road, and roof is 503, 300, 419, and 400 points, respectively.

The threshold values to decide the changed area were then determined on the basis of the value, which is mean ($\pm$N times of standard deviation. Fig. 3 shows histogram curve showing mean and a one-standard deviation threshold used to extract changed area.

The predetermined value of change image was compared with the calculated value of threshold. Zero or one is assigned to all pixels depending on the result of comparison. Namely, all pixels are assigned by zero if the value of change image is less than the threshold and then, are considered as a no changed area. Because the image developed by adopting the threshold is binary, all pixels are classified into one of the changed or no changed areas depending on their value. The samples from high way, whose property was identified by referring the digital map produced previously, were used to evaluate the consistency of the classification results.

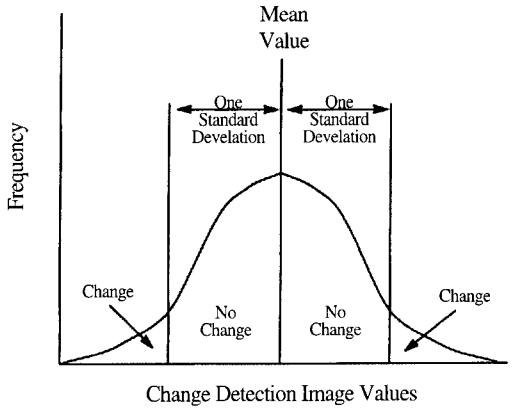

Fig. 3. Histogram curve showing mean and a one-standard deviation threshold used to extract areas of change.

The image rationing scheme was also applied for the extraction of paddy field from the seasonal images acquired at March and June 2001. There was a significant difference in the reflectance of paddy field between the image acquired on March and that on June. The difference of reflection, however, was not significant in seasonal images from any other land covers. Since the reflectance of paddy field depends upon its growth stage and cultivating pattern, the image of March shows higher reflectance of paddy field than that of June. The numerator of image rationing in Eq. (2) is carried out by subtraction of the higher reflectance with the lower one. Initial value of N was -3.0 standard deviations, because a rate of the pixel with lower value than -3.0 standard deviations was only less than 2% of sample numbers.

And then the value of N was increased with an interval of 0.5 and used to assign zero or one to make a binary image. Based on the binary image, the area

change in season was detected.

4. Results and Discussions

1) Pre-processing and Standardization

Through GCP collection, the root-mean-squared errors (RMSE) of three satellite images acquired on March 2000, March 2001, and June 2001 were 0.64, 0.68 and 0.68 pixel, respectively, and they are equivalent to the spatial error less than ± 1.0 pixel (as a reference, pixel size of EOC is ± 6.6m). Table 2 summarizes the basic statistics of the control sets. Comparing the average value of DN (digital number) in Table 2, it was found that the distribution of DN values of the control set was different along the acquired dates satellite image in spite of the selection of the control set features having the property of little change with time. Fig. 4 shows the scatter plot of the control set for March 2000 and March 2001. By applying a linear regression relationship between features of the control set obtained at different dates, the regression equation was obtained:

$$[March2000] \cong [March2001]^T = 1.17 \times [March2001] - 22.6 \quad (3)$$

A linear relationship was also applied to the control sets obtained on March 2001 and June 2001 to identify the difference of DN distribution according to seasonal change (see Fig. 3). A regression equation was determined:

$$[June2001] \cong [March2001]^T = 2.05 \times [March2001] - 61.7 \quad (4)$$

For the annual images, Fig. 5(a) shows that there exists the difference between the average DN values of the four features of the two control sets acquired on the March of 2000 and 2001. By establishing the standardization, the gap between the two control sets, however, disappeared as shown in Fig. 5(b). The average difference between the mean values of each control set feature is minimized from 10.3 to 1.7. Regarding to the seasonal images, the standardization was performed to match the control sets obtained from the image of March 2001 and June 2001. As shown in Fig. 5(c) and Fig. 5(d), DN values of the control set features on June are consistent with that on March in 2001. The average difference between the mean values of each control set feature is minimized from 16.9 to 1.4 for the Fig. 5(c) and Fig. 5(d).

2) Change Detection Using Annual Data

In this paper, the annual change image (ACI) defined

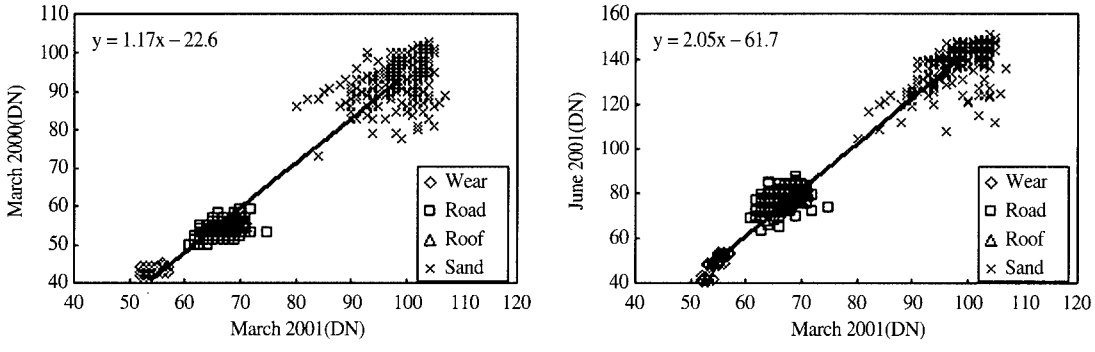

(a) Annual Image (b) Seasonal Image

Fig. 4. Scatter plots of control sets collected from two different dates and equation based on linear regression relationship between mean values for each feature of control sets.

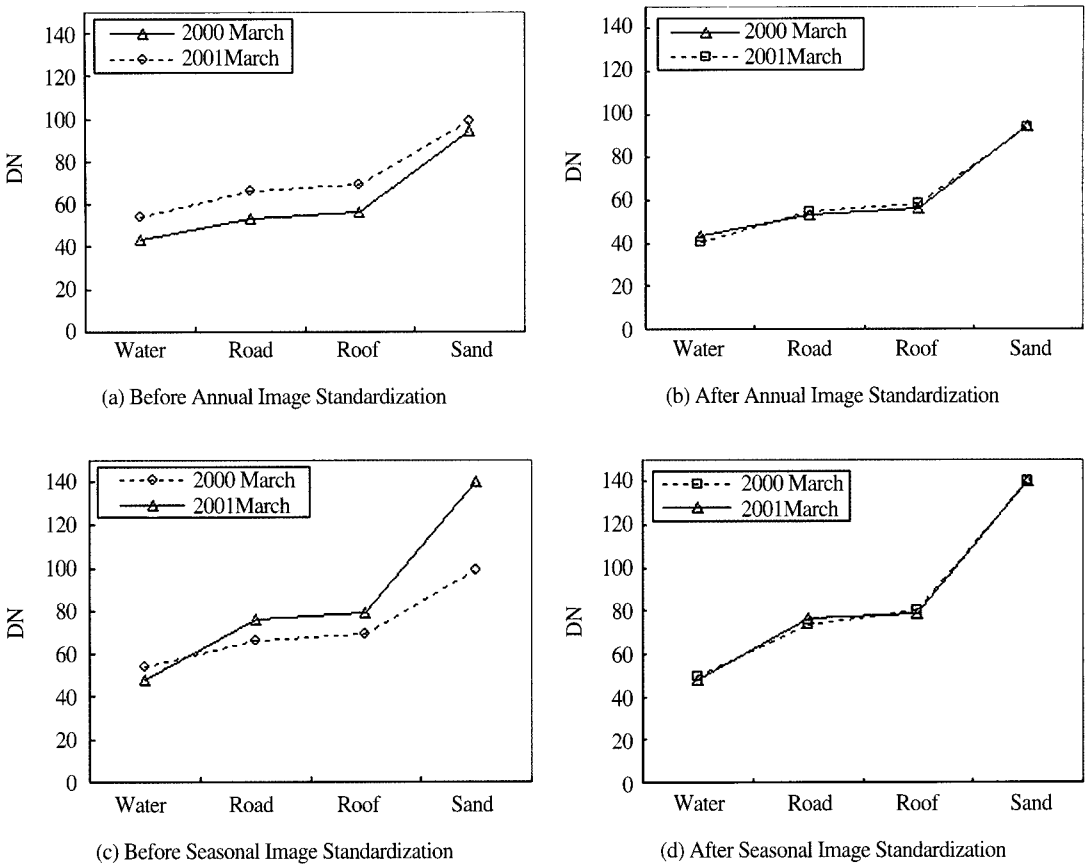

(a) Before Annual Image Standardization

(b) After Annual Image Standardization

(c) Before Seasonal Image Standardization

(d) After Seasonal Image Standardization

Fig. 5. Comparison of mean values of control set before and after applying standardization.

by Eq. (5) was used for detecting annual changes.

$$ACI = \frac{[March2001] - [March2000]}{[March2001] + [March2000]} \quad (5)$$

Table 3 summarizes the result of the accuracy evaluation of the change area detection. To estimate the accuracy of change detection, two sample areas were selected: one was a concrete paved highway area as the invariant feature and the other one was the area of road on going construction as a rapidly changed area in the same image domain of ACI. Next, the total number of sample pixels for not only highway but also the road on going construction. As shown in Table 3, ACI values for all pixels of highway area were compared with the value of threshold that was defined as a function of the standard deviation of ACI values. Namely, an arbitrary value of the threshold was selected first and, then, the absolute value of the threshold was determined as a pivot to assign a binary value of zero or one onto the pixel depending on the ACI value of certain pixel. If ACI value was less than the pivot value, zero was assigned. And if ACI value of the certain pixel was greater than the pivot value, one value was assigned. That means the certain pixel was evaluated to the changed area even though concrete paved highway area was selected as an invariant feature. In the next, the total number of pixels having one value should be counted. And then, it had to be compared with the total number of highway sample because highway should have zero value. As a result, the error rate of 'no changed area' in

Table 3. Result of change area detection by applying threshold range of standard deviation of ACI value.

Threshold Range	No Change Area*1		Change Area*2		Error rate*5
	No. of Pixel*3	Error rate	No. of Pixel*4	Error rate	
ACI*6 > Abs (0.5σ)	1305	98.2%	5	0.5%	59.4%
ACI > Abs (1.0σ)	1189	89.5%	13	1.4%	45.5%
ACI > Abs (1.5σ)	712	53.6%	27	2.8%	28.2%
ACI > Abs (2.0σ)	237	17.8%	72	7.5%	12.7%
ACI > Abs (2.5σ)	20	1.5%	168	17.5%	9.5%
ACI > Abs (3.0σ)	1	0.2%	295	30.7%	15.5%

*1 The sample data of 'No Change Area' were acquired with highway area. The total number of pixel is 1329.
*2 The sample data of 'Change Area' were acquired with rapidly changed area during study period. The total number of pixel is 962.
*3 The number of pixel that is detected to change area out of the total number of pixel to the highway
*4 The number of pixel that is included to changed area from the reference data collected to changed area.
*5 Average value of two error rate of no changed area and changed area.
*6 ACI : Annual Change Image.

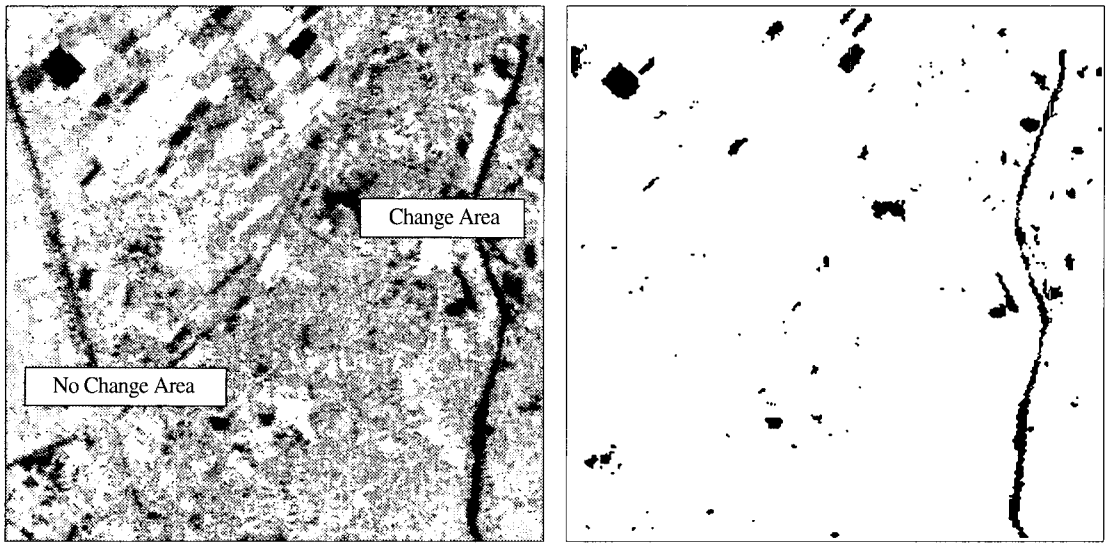

Study area ACI > |2.5σ|

Fig. 6. (a) ACI of study area for the annual change detection, (b) the result image of the optimal threshold (ACI > |2.5σ|) applied.

Table 3 was determined. On the other hand, with same manner, the error rate for the changed area was also determined. The error rate locating on the most right column in Table 3 denoted the average value of the two errors obtained from the sample of highway as no changed area and one of road construction site as a rapidly changed area.

On the basis of the average error rate in Table 3, it was clear that the highest accuracy of detection was achieved when absolute value of 2.5 times of standard deviation of annual change image (ACI) was used as a threshold. Fig. 6 (a) shows the sample images used to evaluate the accuracy of annual change area detection. Fig. 6 (b) shows the result image of the optimal threshold (ACI > |2.5σ|) applied.

Table 4. Result of paddy field extraction by applying threshold range of standard deviation of SCI value.
(Number of pixel (%))

Threshold Range	Paddy Area*1		Other features*2		Total Accuracy*5
	No. of Pixel*3	Accuracy	No. of Pixel*4	Accuracy	
SCI*6 < -3.0	22	1.2%	0	0%	1.2%
SCI < -2.5	137	7.3%	0	0%	7.3%
SCI < -2.0	381	20.2%	0	0%	20.2%
SCI < -1.5	924	48.0%	0	0%	48.0%
SCI < -1.0	1584	84.0%	56	5.0%	79.0%
SCI < -0.5	1869	99.2%	98	8.5%	90.7%
SCI < 0.0	1885	100%	125	10.6%	89.4%

*1 The number of pixel used for paddy is 1885.
*2 This includes urban, water, and forest area. The number of pixel for urban, water, and forest are 1585, 1123, and 525.
*3 Number of pixel detected to paddy from paddy sample data
*4 Number of pixel correctly detected to other features
*5 Result value of two accuracy value's subtraction
*6 SCI : Seasonal Change Image

Referenced Digital Map　　SCI > - 0.5σ

Fig. 7. (a) Referenced digital map used in paddy field extraction, (b) the result image of the optimal threshold (SCI > - 0.5σ) applied.

3) Extraction of Paddy Field Using Seasonal Data

The extraction of paddy field was conducted using the seasonal data of March and June. To discriminate the paddy area from other land cover features such as urban, water, and forest, the seasonal change image (SCI) defined by Eq. (6) was applied.

$$SCI = \frac{[June2001] - [March2001]}{[June2001] + [March2001]} \quad (6)$$

Note that the radiance of paddy field obtained on March is higher than that on June because of growing stage of paddy. Consequently, SCI value of paddy field

defined by Eq. (6) would be negative.

The sample data to evaluate the estimation accuracy was collected from the digital map referenced (Fig. 7 (a)). After applying the threshold, all pixels of SCI were assigned to binary value of zero or one. If the pixel value of SCI is in the range of the applied threshold, the pixel will have identifier of one elsewhere zero will be assigned (e.g. '1' = paddy, '0' = other features). The accuracy of paddy area was calculated by counting the number of correctly detected pixel to paddy from sample paddy data. The accuracy of other features was calculated by the same way of the paddy area. Total accuracy is calculated by averaging the two accuracies in terms of pixels correctly estimated. As a result, the threshold of (SCI < 0.5σ) showed the best performance as shown in Fig. 7 (b) and described in Table 4.

5. Conclusions

Temporally acquired EOC images were used to detect the annually changed area and paddy field. Using the control set consisted of four invariant features such as sand, water, road, and house roofs, atmospheric effects resulted from the difference of acquisition date were removed. A formula of annual change image (ACI) was defined to enhance the image difference between the standardized images obtained in different year. In addition, threshold value was defined as a function of standard deviation of all the ACI value to discriminate the annually changed area. The absolute value of 2.5 times of the standard deviation of ACI values was decided as an optimal threshold in the detection of annual change with 81%. On the other hand, seasonal change image (SCI) was also defined and used to identify paddy field. The optimal threshold was -0.5 times of the standard deviation of SCI with 90.7%.

Acknowledgements

This study is a result of the project funded by Ministry of Science and Technology (MOST), Korea (project code: 99-J-MS-03-B-01-A3). The authors wish to thank MOST, Korea Aerospace Research Institute (KARI), and Korea Institute of Geoscience and Mineral Resources.

References

Badwahr, G.D., W.W. Austin, and J.G. Carnes, 1982. A semi-automatic technique for multitemporal classification of a given crop within a Landsat scene, *Pattern Recognition*, 15(3): 217.

Collins, J.B. and C.E. Woodcock, 1996. An assessment of several linear change detection techniques for mapping forest mortality using multitemporal Landsat TM data, *Remote Sens. Environ*, 56: 66-77.

Coppin, P.R. and M.E. Bauer, 1994. Processing if multitemporal Landsat TM Imagery to optimize extraction of forest cover change features, *IEEE Trans. Geosci. Remote Sens.*, 32(4): 918-927.

Gerson, D.J. and L.K. Fehrenbach, 1983. Temporal image normalization, Final Report, *Defense Mapping Agency.*

Hall, F.G., D.E. Strebel. J.E. Nickelson, and S.J. Goetz, 1991. Radiometric rectification: toward a common radiometric response among multidate, multisensor images, *Remote Sens. Environ*, 35: 11-27.

Lee, K.S. and J.H. Kim, 2000. Change analysis of forest area and canopy conditions in Kaesung, North Korea using Landsat, SPOT and KOMPSAT data, *Korean J. Remote Sens.*, 16(4): 327-338.

Piech, K.R., D.W. Gaucher, E.W. Schimminger, and C.W. Rogers, 1978. Photometric calibration of

black-and white imagery, Rome Air Development Center Technical Report, RADC-TR-78-53.

Piech, K.R. and J.E. Walker, 1971. Aerial color analysis of water quality, *J. Surveying Mapping Div.*, ASCE 97: 185.

Piech, K.R. and J.R. Schott, 1974. Atmospheric corrections for satellite water quality studies, Proc. SPIE 51: 1173.

Schott, J.R., C. Salvaggio, and W.J. Volchok, 1988. Radiometric scene normalization using pseudoinvariant features, *Remote Sens. Environ.*, 26: 1-16.

Singh, A., 1989. Digital change detection techniques using remotely sensed data. *Int. J. Remote Sens.*, 10(6): 989-1003.

Slater, P.N., 1980. Remote Sensing, Optics and Optical Systems, Addison-Wesley, Reading, MA.

Teillet, P.M., N.T. O'Neill, A. Kalinauskas, D. Sturgeon, and G. Fedosejevs, 1987. A dynamic regression algorithm for incorporating atmospheric models into image correction procedures, in IGARSS '87: *Remote Sensing: Understanding the Earth as a System*, May, 2: 913.

Caselles, V. and M.J. Kopez Garcia, 1989. An alternative simple approach to estimate atmospheric correction in multitemporal studies, *Int. J. Remote Sens.*, 10: 1127-1134.

Woodcock, C.E., S. Gopal, and W. Albert, 1996. Evaluation of the potential for providing secondary labels in vegetation maps, *Photogramm. Eng. Remote Sens.*, 62: 393-399.